Nanostructured Manganese Dioxide Thin Films prepared by a Novel Self-Assembly Process

PANG SUH CEM*, WEE BOON HONG & CHIN SUK FUN

Department of Chemistry, Faculty of Resource Science and Technology, Universiti Malaysia Sarawak, 94300 Kota Samarahan, Sarawak, Malaysia

ABSTRACT

We have reported herein a novel self-assembly horizontal submersion process for the deposition of nanostructured manganese dioxide thin films on metalized plastic supporting substrates at ambient temperature and pressure. Uniform manganese dioxide thin films were deposited directly onto metallized plastic supporting substrate via the spontaneous assembly of preformed manganese dioxide nanoparticles in the form of stable colloidal suspension. This process affords a facile approach for the deposition of manganese dioxide thin films by simply repeating the submersion process after the prior deposited layer had been air-dried completely. Thin-film deposition process initially occurred through the spontaneous adsorption of manganese dioxide nanoparticles onto specific surface sites of the metalized substrate. Subsequent events of particle growth, clusters formation, and aggregation or self-organization of particle clusters eventually led to the deposition of nanostructured thin films which were nanoparticulate and highly porous in nature. The surface morphological characteristics of deposited thin films were observed to be significantly affected by the duration of submersion and the post-deposition calcination temperature. By modulating and optimizing these parameters, thin films of tailored microstructure could therefore be prepared. Optimized manganese dioxide thin films were observed to exhibit excellent capacitive behavior as evidenced by the almost perfectly rectangular shape of cyclic voltamograms within the potential range of 0.0 to 1.0 V (versus SCE) in mild aqueous Na_2SO_4 electrolyte. The cycling stability and reversibility of these films were evaluated by prolonged charge-discharge cycling and no substantial deterioration of performance in terms of charge capacity and capacitive behaviors were observed after 1000 cycles. We speculate that the high capacitance value exhibited by self-assembled manganese dioxide thin films in mild aqueous electrolyte could be attributed to reversible and homogenous intercalation and deintercalation of protons during the charge and discharge cycling. The potential utility of self-assembled manganese dioxide thin films for the fabrication of electrochemical devices, in particular thin-film electrochemical capacitors is therefore envisaged.

Keywords: *Manganese dioxide, nanoparticles, self-assembly, thin films, electrochemical capacitors.*

INTRODUCTION

The utility of manganese dioxide (MnO_2) as electrode material for the fabrication of primary and secondary electrochemical cells has long been established due to its favorable electrochemical characteristic and inexpensive cost of production (Qu, 2006 and Yagi *et al.*, 2002). In recent decades, intense research interest has been focused on the utilization of MnO_2 as electrode material for the fabrication of pseudocapacitive electrochemical capacitors as it is considered toxicologically benign and cheap. Pang *et al.* (2000) and Chin *et al.* (2002) had demonstrated a specific capacitance

Corresponding author: scpang@frst.unimas.my

of about 700 F/g at 50 mV/s for ultra-thin nanoparticulate manganese dioxide thin films prepared by the sol-gel process, thereby provided further impetus for intensified research on nanoparticulate manganese dioxide thin films. Recent studies have concurred that nanoparticulate manganese dioxide thin films possess favorable electrochemical properties and are promising electrode materials for the fabrication of high power and energy density electrochemical capacitors.

Various chemical routes for the preparation of manganese dioxide thin-film electrodes that are suitable for the fabrication of electrochemical capacitors have been developed recently. Dai *et al.* (2006) prepared

MnO_2 thin films by electrostatic spray deposition from $KMnO_4$ solution and reported a specific capacitance of 163 F/g at scan rate of 5 mV/s in 0.2M Na_2SO_4. Nanostructured manganese dioxide that was prepared by the sonochemical method had achieved a specific capacitance of 344 F/g at scan rate of 5 mV/s in 0.5M Na_2SO_4 electrolyte (Zolfaghari *et al.*, 2007). Cathodic electrodeposited MnO_x was reported to exhibit a specific capacitance of 425 F/g at scan rate of 10 mV/s in 0.25M Na_2SO_4 electrolyte (Nagarajan *et al.*, 2006). Potentiodynamical anodic co-deposited manganese oxide/carbon composite electrode was reported to possess a specific capacitance of 410 F/g at the scan rate of 10 mV/s in 1.0M Na_2SO_4 electrolyte (Liu *et al.*, 2007).

The present paper focuses on the characterization of nanostructured MnO_2 thin films on nickel coated PET substrate prepared by a novel self-assembly approach under controlled conditions. The effect of deposition parameters such as duration of submersion and post-deposition calcination temperature on the microstructure and electrochemical properties of MnO_2 thin films were investigated.

MATERIALS & METHOD

Preparation of MnO$_2$ sol

All chemicals were of analytical grades and were used as obtained without further purification. Stable MnO_2 sol was prepared according to method reported by Perez-Benito et al. (1996) based on the following reaction stoichiometry:

$$8 \, MnO_4^- + 3 \, S_2O_3^{2-} + 2 \, H^+ \rightarrow 8 \, MnO_2 + 6 \, SO_4^{2-} + H_2O$$
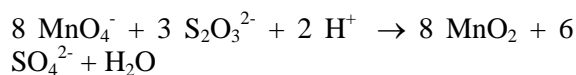
Deposition of MnO$_2$ Thin Films

A thoroughly cleaned nickel-coated PET substrate (3M PP2900) of dimension 40 mm x 44 mm were positioned perfectly horizontal and flat in a glass petri dish with the aid of adhesive tape. MnO_2 sol was then poured slowly into the glass petri dish until the substrate was completely submersed. After the predetermined submersion duration, the sol was then drained out meticulously using a micropipette. The MnO_2 thin film formed spontaneously on the PET substrate was then air-dried under controlled environment.

Nanostructured MnO_2 thin films of varying thicknesses were prepared through layer-by-layer self-assembly by simply repeating the horizontal submersion coating process the desired number of times. The deposited MnO_2 film was left to dry in air overnight prior to heat treatment in a tube furnace at 200 $^{\circ}$C in air for an hour.

Physical and Electrochemical characterization of MnO$_2$ Films

The electroactive material loading and homogeneity of MnO_2 thin film was evaluated by atomic adsorption spectroscopy (AAS). The electrodes were dissolved in the H_2O_2/HNO_3 mixture solution and the concentration of Mn per unit volume (cm^3) was determined using atomic absorption spectroscopy (AAS). The electroactive material loading of MnO_2 thin-film electrode (mass per unit area (g/cm^2)) was calculated based on the Mn concentration as determined using the formula weight of stoichiometric MnO_2 of 86.94 g/mol.

The surface morphology of the MnO_2 thin films was observed using a field emission scanning electron microscope (FESEM, LEO 1525), whereas their impedance and capacitive behaviors were investigated by cyclic voltammetry (CV) and electrochemical impedance spectroscopy (EIS) operated on a computer interfaced Frequency Response Analyzer (PARSTAT 2263). Cyclic voltammetry (CV) studies were performed in 1.0M Na_2SO_4 aqueous electrolyte using a standard 3-electrode configuration with platinum foil as the counter electrode and Saturated Calomel Electrode (SCE) fitted with a Vycor frit as the reference electrode. The surface area of the working electrodes was fixed at 0.126 cm^2 and a scan rate of 50 mV/s within potential window of 0 – 1.0V (vs SCE) was used. The specific capacitance (SC) of the MnO_2 thin films was calculated by dividing the integrated anodic current (Q_a) with the mass of electroactive material on electrode (*m*) and the width of potential scan window (ΔV) according to equation (1).

$$Specific \; Capacitance \; (SC) \; = \; \frac{1}{m\Delta V} \int I \delta t \quad (1)$$

Electrochemical impedance spectroscopy (EIS) measurements for MnO_2 thin-film electrodes were performed within the frequency range of 1 MHz to 10 mHz. The impedances at 100 mHz and 10 mHz were used for capacitance (C) calculation according to equation (2).

$$\text{Capacitance, } C = - \frac{1}{\omega Z_{img}} \qquad (2)$$

where, C is the capacitance, ω $(=2\pi f)$ is the angular frequency and Z_{img} is the imaginary part of the impedance. Specific capacitance (SC) was calculated based on the capacitance values divided by the mass of electroactive material on the electrode.

RESULTS & DISCUSSION

Characterization of MnO₂ Thin Films

Field Emission Scanning Electron Microscopy

Figure 1 shows SEM micrographs of MnO_2 thin films deposited on the nickel- coated PET substrates by the novel self-assembly horizontal submersion process. All SEM micrographs showed that MnO_2 thin films were nanoparticulate in nature with particle size ranged between 30 to 50 nm. Considerably large variation in pores sizes ranging from macropores to micropores were visually discernible and hence indicative of the porous nature of these films. However, MnO_2 thin films prepared by repeating the deposition process with different number of times (3-5x) showed slightly increased film density and uniformity (Figure 1(b) and (c)). We speculate that the MnO_2 film deposition process was being catalyzed by active sites available on the surface of nickel-coated PET substrate. This film deposition process was essentially a spontaneous self-assembly process which involved initial adsorption of manganese dioxide nanoparticles onto surface active sites of the metallized supporting substrate, subsequent particle growth, clusters formation, and aggregation of clusters, and eventually led to the deposition of nanostructured MnO_2 thin film on the supporting substrate.

Figure 2 shows SEM micrographs of various MnO_2 thin films of different coatings before and after heat treatment at 200 °C in air for an hour. MnO_2 films generally showed increase in their film density and notably reduced aggregate sizes upon heat treatment, with thinner films (1 coating) showed comparatively higher degree of densification than that of thicker films (5 coatings).
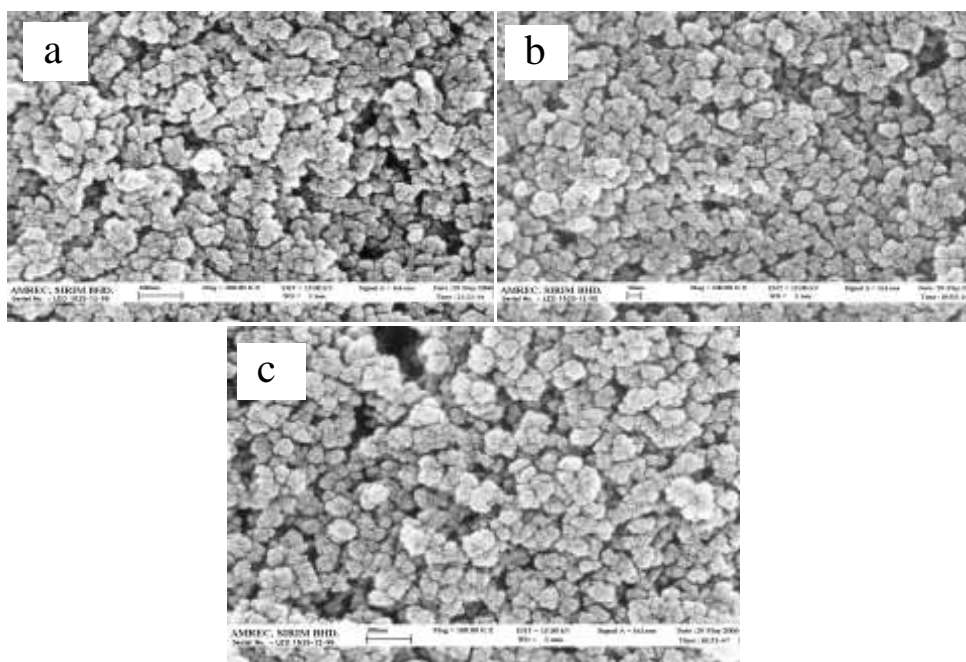

Figure 1. SEM micrographs of MnO_2 films deposited on nickel-coated PET substrate prepared by repeating the self-assembly horizontal submersion process (a) 1x; (b) 3x, and (c) 5x. (Magnification: 100,000 x)
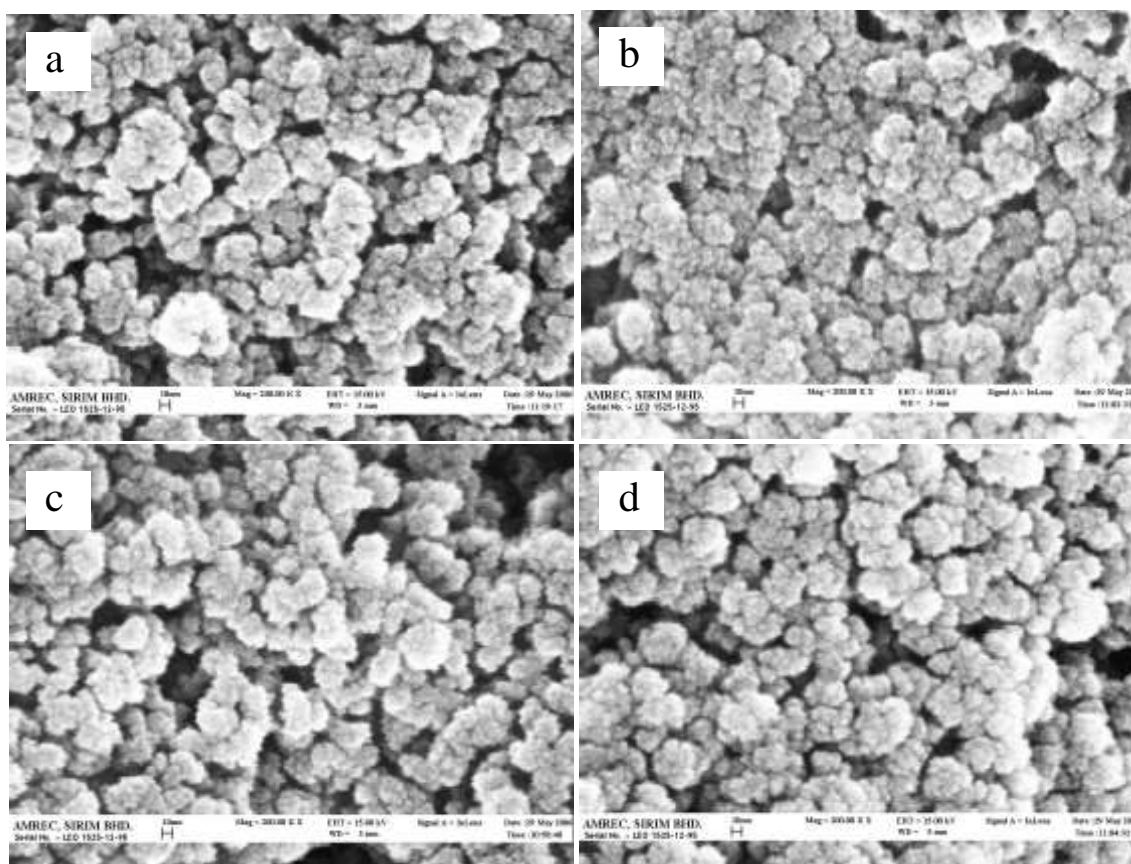
Figure 2. SEM micrographs of MnO$_2$ thin films before and after heat treatment; (a) 1x before, (b) 1x after, (c) 5x before, and (d) 5x after (Magnification: 200,000 x).

All self-assembled MnO$_2$ thin films showed good adhesion to the nickel-coated PET substrates even without the use of any binders. However, cracks were observed (at low magnification) on most film surfaces after heat treatment which could be attributed to film densification. Nonetheless, the highly porous nature of these films would facilitate facile accessibility of electrolyte ions into the bulk of the electrode materials during voltammetric cycling. The heat treatment could have effectively removed all physisorbed water and a substantial portion of chemisorbed water resulting in the densification of MnO$_2$ thin films. The predominant advantage of film densification through heat treatment process was to afford enhanced electronic connectivity and conductivity between nanoclusters thereby contributed to substantial reduction of the internal resistance of films. Lower internal resistance of MnO$_2$ films correlated directly to higher electrical conductivity, which in turn, augments their pseudocapacitive performance favorable for the fabrication of charge-storage devices. Besides, the presence of excess chemically bound structural water could perform a pivotal role in aiding the cationic/electrolyte accessibility in MnO$_2$ films (Lee *et al.*, 1999). Henceforth, an optimal balance between the effect of densification on reducing internal electrical resistance and the structural water content in the bulk electroactive material for promoting cationic diffusivity should be attained in order to achieve optimized pseudocapacitive performance.

The morphological structure of bulk electroactive material could substantially influence the accessibility of cations into internal surfaces of the electrode material. The smaller the pore sizes of the electroactive materials, the larger is its surface area and thence affords higher charge storage capacity. However, the pore size must be large enough for the intercalation of cations into the bulk of the electroactive material. Preparation of electroactive materials with desired pore size

distribution has always been a very challenging task.

Atomic Absorption Spectroscopy (AAS)

In order to corroborate the homogeneity and uniformity of self-assembled MnO_2 thin films, each selected thin film electrode was being cut into four smaller portions of same dimensions. These films were being dissolved in the H_2O_2/HNO_3 mixture and the Mn concentrations were determined quantitatively using AAS. The total mean MnO_2 loading of films were calculated to be 0.1029 mg/cm^2 based on the concentration of Mn determined. Comparison between MnO_2 loadings for these four smaller electrode portions showed good agreement

which was deemed sufficient to substantiate the homogeneity and uniformity of deposited MnO_2 thin films.

Cyclic voltammetry (CV)

Figure 3 shows the cyclic voltammograms of MnO_2 thin-film electrodes with almost rectangular shape indicating good capacitive behaviors. The areas within these CV curves were observed to increase substantially with increased number of coatings by repeating the horizontal submersion process. This indicated that the charge capacity of deposited MnO_2 films increased with their relative film thickness.
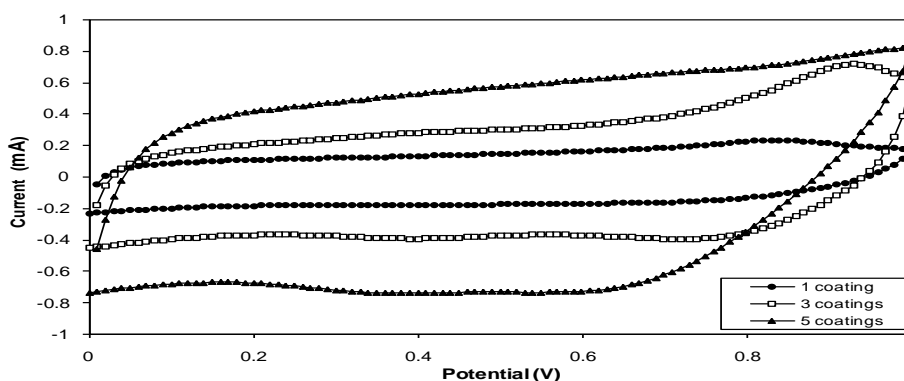

Figure 3. Cyclic voltammograms of MnO_2 thin films prepared with different number of coatings and relative film thicknesses.

Figure 4 shows the effect of number of coatings on the charge capacity (mF/cm^2) and Q_a/Q_c ratio of MnO_2 thin films. A positive linear correlation was observed between the charge capacity values and the number of

coatings or relative film thicknesses. The Q_a/Q_c ratios were approximately unity which indicated excellent reversibility of the charge/discharge processes that occurred within these MnO_2 thin-film electrodes.
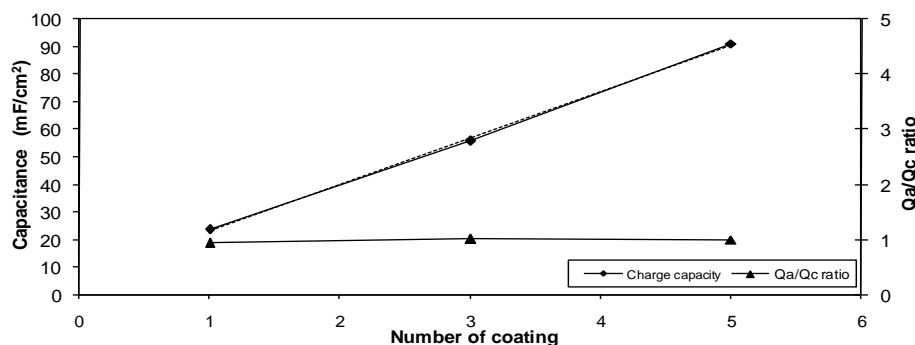

Figure 4. Effect of number of coatings on the electrochemical properties of self-assembled MnO_2 thin films.

Performance Evaluation of Thin-film Electrochemical Capacitor Prototypes

Cyclic voltammograms of electrochemical capacitor prototypes with different electrode configurations were being evaluated in 0.2 M Na_2SO_4 liquid electrolyte and agar-based gel electrolyte containing dissolved 0.2 M Na_2SO_4 are as depicted in Figures 5 – 8.
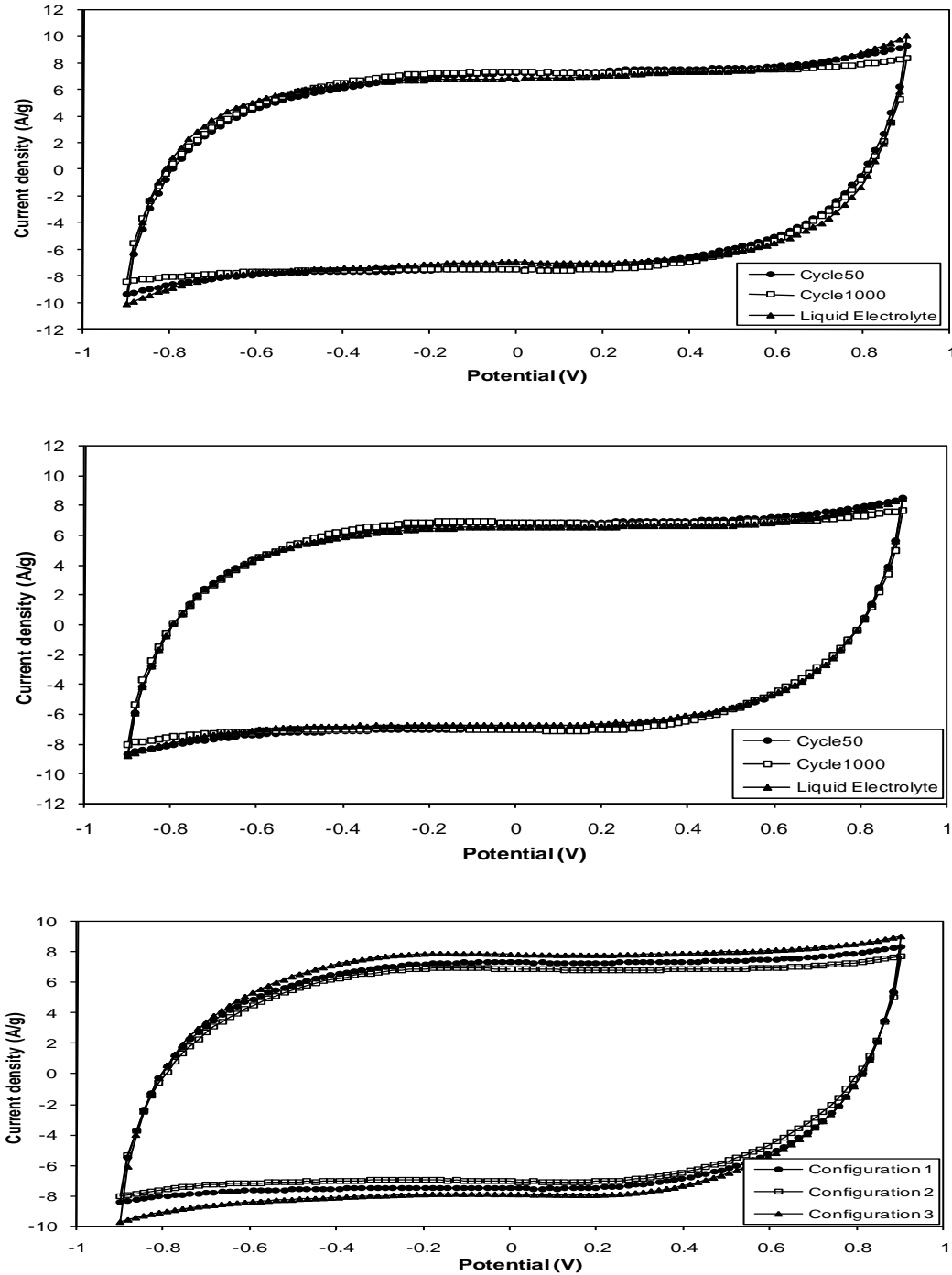

Figure 5. Cyclic voltammograms of prototype thin-film electrochemical capacitor with different electrode configurations, (a) Configuration 1, (b) Configuration 2, and (c) Comparison between electrode configuration 1,2 & 3. Cycles 50 and 1000 were obtained with all prototypes in agar-based gel electrolyte.

All electrochemical capacitor prototypes with different device configurations were observed to exhibit excellent capacitive behaviors as evidenced by the almost perfectly rectangular shape of CV curves at the scan rate of 50 mV/s within the potential window of -0.9 V to 0.9 V. No redox peaks were discernible within these CV curves even after prolong cycling test of exceeding 1,000 cycles, which could be attributed to high phase stability and reversibility of the pseudocapacitive electrochemical reactions occurring within these prototype devices.

Figure 6 shows the cycling behaviors of electrochemical capacitor prototypes with different electrode configurations. The maximum specific capacitance achieved for all these prototypes ranged between 123 F/g and 141 F/g. All prototypes exhibited excellent cycling stability without showing any loss in their capacitance, albeit an overall capacitance increment of about 2 to 4% upon cycling for 1,000 cycles was observed indicating that prototypes fabricated in this study were electrochemically stable. The long-term stability of eletroactive thin-film electrode material is the most substantial criterion for electrochemical capacitor application.
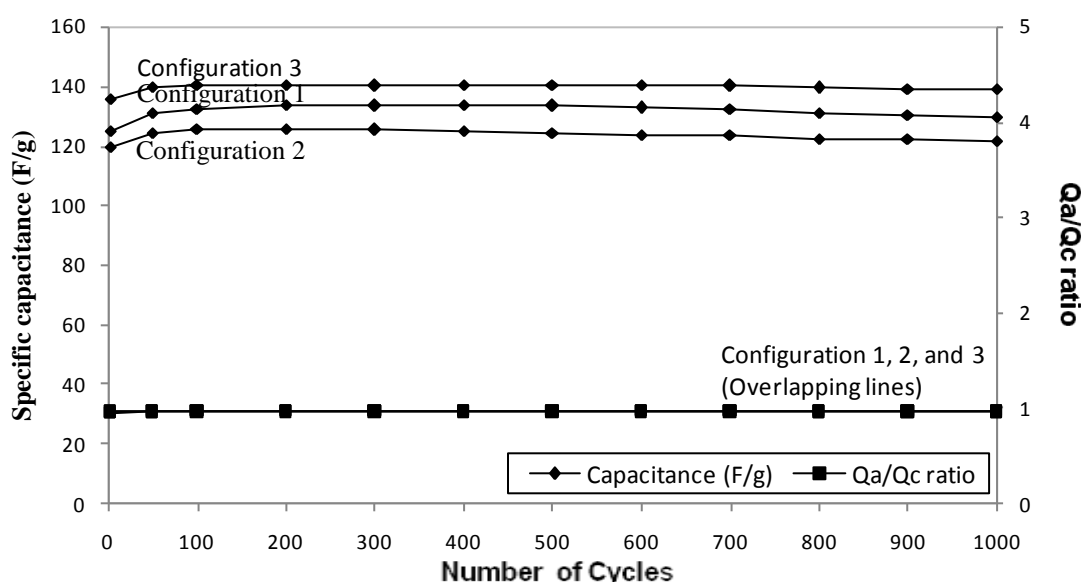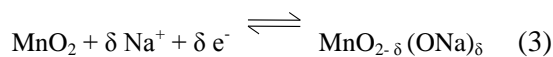

Figure 6. Cycling behaviors of electrochemical capacitor prototypes with different electrode configurations.

The observed excellent cycling stability of the MnO_2 thin films for exceeding 1,000 cycles showed that there was no occurrence of structural modification and dissolution of active material throughout the prolong charge and discharge cycling test. We speculate that such high cycling stability and reversibility could be attributed to the amorphous nature of these films as well as the optimal scan potential window within the range of -0.9 V to 0.9 V which had collectively prevented over-charging or over-discharging the prototype devices.

The specific capacitance of MnO_2 thin films is believed to be predominantly contributed by pseudocapacitive behavior as a result of reversible redox reaction which corresponds to the reduction of MnO_2. Double layer capacitance might have inconsequential effect upon the overall capacitance of these prototypes and was therefore neglected in this study. According to Wen *et al*., (2004), the charge storage mechanism of MnO_2 involves rapid and reversible faradaic reaction through the cationic and protonic exchange. The redox processes for both Na^+ and H^+ ions which are present in the electrolytes could be shown in equations (3) and (4):

$$MnO_2 + \delta\, Na^+ + \delta\, e^- \rightleftharpoons MnO_{2-\delta}(ONa)_\delta \quad (3)$$

$$MnO_2 + \delta\, H^+ + \delta\, e^- \rightleftharpoons MnO_{2-\delta}(OH)_\delta \quad (4)$$

The pseudocapacitance of a redox electrochemical capacitor might have been due to the amorphous nature of its electroactive material that constitutes the electrodes (Lee *et al.*, 1999). This could plausibly explain that the capacitance of MnO_2 thin films prepared in the present study was attributed to its amorphous nature and porosity which collectively enabled high accessibility of Na^+ ions into the internal surfaces of these thin films. It is noteworthy to emphasize that factors which could significantly influence the rate of charging/discharging process of MnO_2 and consequently the capacitance of the electrochemical capacitors include the size of both the cations and the hydration sphere of the cations in the electrolyte, the concentration of cations, the mobility of cations, the rate of adsorption/desorption of cations at the electrode surface and the pore size of the electroactive material (Wen *et al.*, 2004). Lee *et al.* (1999) also reported that the pseudocapacitative performance of both electroactive materials, $K_xMnO_{2+\delta}.nH_2O$ and amorphous MnO_2 was attributed to the K^+ ions which served as the working ions in complementary to the chemisorption and desorption of protons.

Considering the charge-storage mechanism that involves a total reduction of Mn^{4+} to Mn^{3+}, such a redox reaction would contribute a theoretical specific capacitance of about 1,200 F/g. This specific capacitance value is approximately one order of magnitude larger than those values obtained in our prototype devices. However, this theoretical value has never been attained thus far and the average specific capacitance reported for MnO_2 electrode tested in aqueous electrolyte is merely 160 F/g (Brousse *et al.,* 2006). Specific capacitance values achieved for our electrochemical capacitor prototypes were well within the same order of magnitude as the reported average value. Among parameters which might have significant influences upon the capacitive performance of the electrochemical capacitors include electrode design, type of electrolyte used, current collector, water content in the electrode material, pore size distribution, microstructure of MnO_2, and Mn(III)/Mn(IV) ratio in the starting material.

Electrochemical impedance spectroscopy (EIS)

Figure 7 and Table 1 show the typical layout and dimensions of supercapacitor prototypes with three different electrode configurations. Configuration 1 comprised an identical pair of electrodes positioned horizontally with an interelectrode gap distance of 0.1 mm. Both EC prototypes of configuration 2 and 3 comprise interdigitated array (IDA) electrodes of different electrode array lengths and widths. These prototypes of dual-planar thin-film electrochemical capacitors on flexible metalized PET substrate were fabricated using a novel cost-effective rapid prototyping process according to the desired electrode configurations. In this study, functional supercapacitor prototypes were fabricated with either 0.2 M Na_2SO_4 aqueous electrolyte or by depositing a thin layer of agar-based gel electrolyte containing 0.2 M Na_2SO_4 solution directly onto the MnO_2 thin-film electrodes. IDA electrode configuration offers many pronounced advantages compared to the typical parallel electrodes which include rapid attainment of steady-state current, higher current collection efficiency, rapid redox reaction kinetic, higher detection sensitivity and selectivity, smaller charging current and smaller potential (iR) drop.
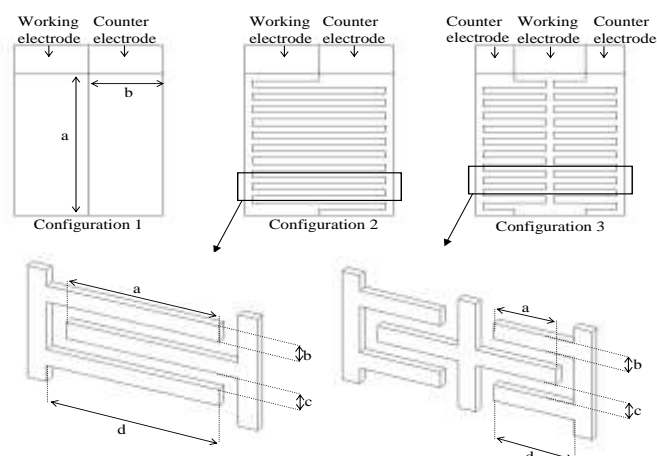
Figure 7. Layout of electrochemical capacitor prototypes of three different electrode configurations. (a) length of array electrode pair; (b) array electrode width; (c) interelectrode gap distance, and (d) length of individual array electrode.

The Nyquist plots for electrochemical capacitor prototypes of different electrode configurations being evaluated in different electrolyte media (liquid or agar-based gel electrolytes) are shown in Figures 8(a) - (h). EIS is a consequential and vastly applicable electrochemical characterization technique for any electrochemical cells, particularly electrochemical capacitors. The impedance plot for an ideal capacitor is a vertical line parallel to the imaginary impedance axis. Impedance plots which showed a steep slope in the low frequency region and a semicircular curve in the high frequency region were indicative of capacitive behaviors of typical electrochemical capacitors. Based on the Nyquist plots for all electrochemical capacitor prototypes, several types of resistances that could be identified at the high frequency range include contact resistance R_c at the MnO_2 active material/nickel current collector interface, electrolyte resistance R_s, and MnO_2 electrode resistance R_e. The capacitance C of the electrochemical capacitor prototypes could be derived from the low frequency regions of 100 mHz and 10 mHz using equation (2).

Table 1. Typical layout dimension for electrochemical capacitor prototypes of various electrode configurations.

| Prototype Configuration	Dimension (mm)			
	a	b	c	d
C1	16.0	5.0	0.1	N/A
C2	7.8	1.0	0.1	7.9
C3	3.3	1.0	0.1	3.4

Key: "N/A" indicates not applicable.

As shown in Figure 8, all electrochemical capacitor prototypes exhibited typical semicircular and steep vertical impedance responses in the high and low frequency regions, respectively. Prototypes with liquid electrolyte (0.2 M Na_2SO_4) and agar-based gel impedance plots for prototypes with agar-based gel electrolyte were observed to have shifted slightly to higher real impedance Z_{real} as compared to that of liquid electrolyte. Figures 9(d) – (f), showed distinctive shift of the impedance plots particularly in the lower frequency regions for agar-based gel electrolyte prototypes before and after voltammetric cycling test. In addition, the semicircular impedance responses at higher frequency regions after cycling test were not as pronounced as those before long-term cycling test. These responses could be attributed to microstructural changes of electroactive material which ameliorates penetration of electrolyte into the recess area of the electrode materials. Figures 8(g) and (h) shows the Nyquist plots of prototypes in liquid electrolyte before long-term cycling test and prototypes in agar-based gel electrolyte after long-term cycling test, respectively. Both insets clearly showed the substantially diminished semicircular impedance plots for prototypes in agar-based gel electrolyte.

Polymer gel electrolyte constituting of polysaccharide such as agar gel containing dissolved salt could indeed replace liquid-based electrolyte in the fabrication of all-solid-state electrochemical capacitor (Mochizuki et al., 2004). Results of EIS analysis have shown that agar-based polymer gel electrolyte (1 % w/v) with dissolved Na_2SO_4 salt exhibited comparable ionic conductivity with that of 0.2 M Na_2SO_4 liquid electrolyte. This could be attributed to similarity in the molecular diffusivity for both polysaccharide-based gel electrolyte and liquid electrolyte. In order for polymer gel electrolyte to perform equally well as liquid electrolyte, we speculate that the amount of electrolyte being encapsulated within pores of polymer gel electrolyte should be taken into account. It has been established that the amount of water or electrolyte plays a pivotal role in enhancing cationic intercalation into the bulk of the electroactive material electrolyte containing dissolved salt (0.2 M Na_2SO_4) did not show any distinctive differences in the electrolyte resistance R_s at high frequency regions (Figure 9(a)-(c) insets).

However, based on the EIS data, the highest specific capacitance calculated at the lower frequency range for prototypes of configurations C1, C2, and C3 and packaged separately with gel electrolyte were determined to be 133 F/g, 125 F/g, and 152 F/g, respectively. Specific capacitance values for electrochemical capacitor prototypes constructed with gel electrolyte were observed to be generally higher by about 15 to 30 F/g after long-term cycling test. These results were observed to agree closely with specific capacitance values obtained by the cyclic voltammetry technique.
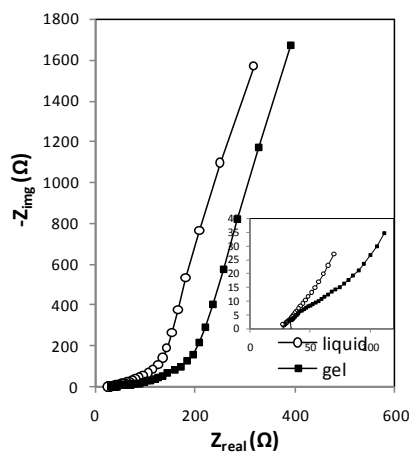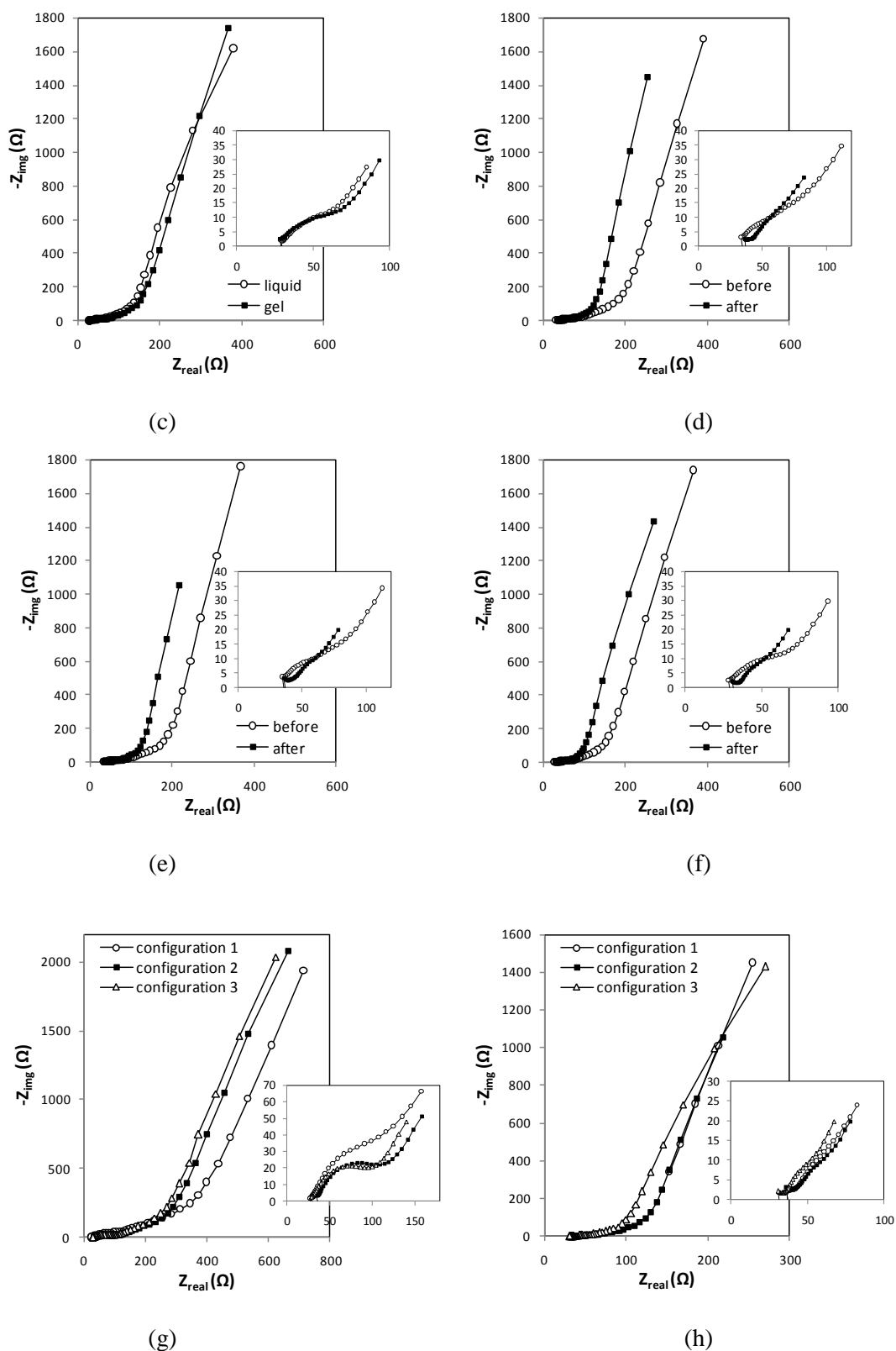

(a)
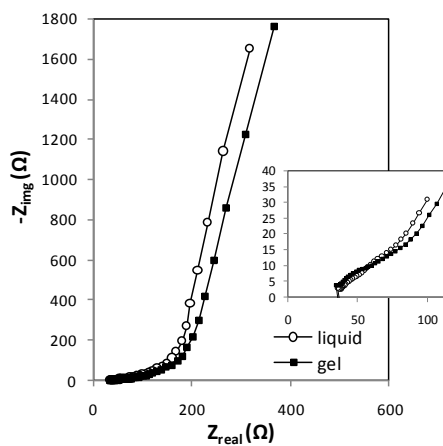
(b)

Figure 8. Nyquist plots of various electrochemical capacitor prototypes, (a) C1, liquid and gel, (b) C2, liquid and gel, (c) C3, liquid and gel, (d) C1, gel, before & after cycling, (e) C2, gel, before & after cycling, (f) C3, gel, before & after cycling, (g) C1,2,3, liquid, before cycling, and (h) C1,2,3, gel, after cycling. All prototypes were tested at ambient temperature and 100%RH within the frequency range of 1 MHz to 10 mHz. C: configuration; Electrolyte: Na_2SO_4 (liquid) electrolyte; Agar-based (gel) electrolyte.

CONCLUSION

Nanostructured manganese dioxide thin films prepared by a novel self-assembly process were nanoparticulate and highly porous in nature. The microstructure and electrochemical properties of these self-assembled films could be tailored through optimization of the deposition parameters and conditions. Self-assembled manganese dioxide thin films exhibited excellent capacitive behavior with high cycling stability and reversibility for exceeding 1,000 charge-discharge cycles. As such, self-assembled manganese dioxide thin films are very promising electrode materials for the fabrication of high power and energy density thin-film electrochemical capacitors.

ACKNOWLEDGEMENTS

REFERENCES

Brousse, T., Toupin, M., Dugas, R., Athouel. L., Crosnier, O., & Bèlanger, D. (2006). Crystalline MnO_2 as Possible Alternatives to Amorphous Compounds in Electrochemical Supercapacitors. *Journal of the Electrochemical Society, 153 (12)*: A2171 - A2180.

Chin, S. F. Pang S. C., & Anderson M.A. (2002). Material and Electrochemical Characterization of Tetrapropylammonium Manganese Oxide Thin Film as Novel Electrode Materials for Electrochemical Capacitors. *Journal of Electrochemical Society*, 149(4): A379 - 384.

Dai, Y., Wang, K., Zhao, J. C., & Xie, J. Y. (2006). Manganese oxide film electrodes prepared by electrostatic spray deposition for electrochemical capacitors from the $KMnO_4$ solution. *Journal of Power Sources, 161*: 737 – 742.

Lee, H. Y., Manivannan, V., & Goodenough, J. B. (1999). Electrochemical capacitors with KCl electrolyte. Comptes Rendus de l'Académie des Sciences - Series IIC – Chemistry, 565 – 577.

Liu, E. H., Meng, X. Y., Ding, R., Zhou, J. C., & Tan, S. T. (2007). Potentiodynamical co-deposited manganese oxide/carbon composite for high capacitance electrochemical capacitors. *Materials Letters, 61*: 3486 – 3489.

Mochizuki, N., Ueno, H., & Kaneko, M. (2004). Solid medium for conventional electrochemical measurements. *Electrochimica Acta, 49*: 4143 – 4148.

Nagarajan, N., Humadi, H., & Zhitomirsky, I. (2006). Cathodic electrodeposition of MnO_x films for electrochemical supercapacitors. *Electrochimica Acta, 51*: 3039 – 3045.

Qu, D. Y. (2006). Investigation of the porosity of electrolytic manganese dioxide and its performance as alkaline cathode material. *Journal of Power Sources, 156*: 692 – 699.

Pang S. C., Anderson, M. A. & Chapman, T. W. (2000) Novel Electrode Materials for Thin-Film Ultracapacitors: I. Comparison of Electrochemical Properties of Sol-Gel-Derived and Electrodeposited Manganese Dioxide. *Journal of Electrochemical Society*, 147(2): 444-450.

Perez-Benito, J. F., Arias, C. & Amat, E. (1996). A kinetic study of the reduction of colloidal manganese dioxide by oxalic acid. *Journal of Colloid and Interface Science*, 177: 288-297.

Wen S., Lee, J. W., Yeo, I. H., Park, J. M., & Mho, S. I. (2004). The role of cations of the electrolyte for the pseudocapacitive behavior of metal oxide electrodes, MnO_2 and RuO_2. *Electrochimica Acta, 50*: 849 – 855.

Yagi, H., Ichikawa, T., Hirano, A., Imanishi, N., Ogawa, S., & Takeda, Y. (2002). Electrode characteristics of manganese oxides prepared by reduction method. *Solid State Ionics, 154 -155*: 273 – 278.

Zolfaghari, A., Ataherian, F., Ghaemi, M., & Gholami, A. (2007). Capacitive behavior of nanostructured MnO_2 prepared by sonochemistry method. *Electrochimica Acta, 52*: 2806 – 2814.